Article citation info:
Górzyńska M, Pielecha I. Numerical investigation of pre-chamber holes diameter geometry on combustion parameters in a hydrogen-powered Turbulent Jet Ignition engine. Combustion Engines. 0000;XXX(X):xx-xx. https://doi.org/10.19206/CE-193950

Marcelina GÓRZYŃSKA
Ireneusz PIELECHA

Combustion Engines
Polish Scientific Society of Combustion Engines

Numerical investigation of pre-chamber holes diameter geometry on combustion parameters in a hydrogen-powered Turbulent Jet Ignition engine

ARTICLE INFO

Received: 25 June 2024
Revised: 13 September 2024
Accepted: 30 September 2024
Available online: 11 October 2024

The search for substitutes for conventional fuels leads to the use of non-hydrocarbon fuels or synthetic fuels. One of them is hydrogen. The use of hydrogen in combination with a two-stage charge formation system leads to the combustion of lean ($\lambda > 1$) or very lean ($\lambda > 3$) charges. The simulation tests carried out were aimed at determining the best configuration of the chamber connecting the pre-chamber with the main combustion chamber. Three variants of the diameter of the holes connecting the chambers were selected (d = 0.5; 1.0 and 1.5 mm) in combination with different fuel doses fed to the pre-chamber. A passive chamber (qo_PC = 0 mg) and an active chamber (qo_PC = 0.4 and 1.2 mg) were used with a constant fuel dose to the main chamber (qo_MC = 6 mg). The research was conducted using AVL Fire 2022.1 software using the moving mesh of the LDV engine. Based on the simulation work, the most favourable conditions for conducting the process were determined, taking into account the thermodynamic effects of the process and acceptable levels of nitrogen oxide concentration. The resulting correlation maps of chamber hole sizes and fuel doses supplied to the pre-chamber can serve as a preliminary basis for selecting control options for hydrogen combustion in the TJI system.

Key words: *hydrogen combustion, Turbulent Jet Ignition, pre-chamber, thermodynamic parameters, CFD research*

1. Introduction

In the context of growing environmental concerns and the finite nature of fossil fuel resources, the quest for alternative fuels have become a pivotal focus in the field of automotive and energy engineering. Traditional fossil fuels, while efficient and energy-dense, contribute significantly to greenhouse gas emissions and air pollution, exacerbating climate change and posing serious public health risks. To mitigate these adverse effects, researchers and engineers are increasingly exploring sustainable and cleaner fuel options.

Among the various types of alternative fuels, compressed natural gas (CNG), hydrogen, and ethanol have emerged as prominent contenders. Each of these fuels offers unique advantages and challenges, making them subjects of extensive study and development. CNG, primarily composed of methane, is a cleaner-burning alternative to gasoline and diesel, producing fewer carbon emissions and particulates. Hydrogen, on the other hand, stands out for its potential to produce zero emissions when used in fuel cells or internal combustion engines, emitting only water vapor as a byproduct. Ethanol, derived from biomass, presents a renewable option that can be integrated into existing fuel infrastructures with relative ease.

This study focuses specifically on hydrogen as a fuel, due to its high energy content per unit mass and its potential to significantly reduce the carbon footprint of transportation. The utilization of hydrogen in internal combustion engines (ICEs) and fuel cells represents a promising pathway toward achieving near-zero emissions. However, the adoption of hydrogen-powered engines requires a comprehensive understanding of its combustion characteristics, efficiency, and associated technical challenges.

It is projected [37] that the global market for hydrogen-powered internal combustion engines will reach $35 billion by 2030 and approximately $89 billion by 2040, with a Compound Annual Growth Rate (CAGR) of 9.78% during the forecast period of 2030–2040 (Fig. 1). Hydrogen-powered internal combustion engines (usually modified versions of traditional gasoline engines) will be essential for vehicle propulsion. These engines, utilizing new technologies (e.g., two-stage combustion – TJI), can offer near-zero emissions while simultaneously promoting the development of hydrogen infrastructure worldwide.

The major players operating in the hydrogen combustion engine market are Honda, Toyota, Komatsu, JCB, BMW, MAN and others. The market for hydrogen internal combustion engines is rapidly growing due to swift research and development, as well as the use of hydrogen as a clean fuel. This growth is further driven by an increasing number of government initiatives aimed at promoting the use of fuel cell vehicles, which in turn fuels the market for hydrogen internal combustion engines.

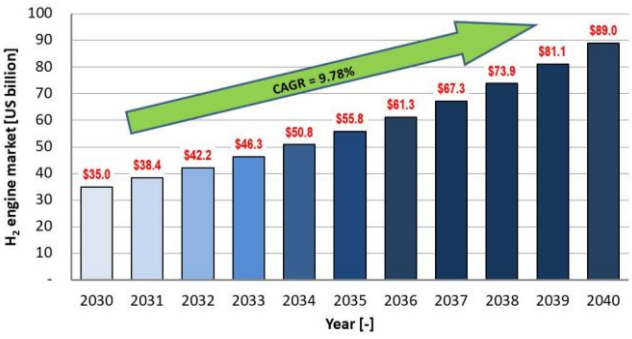

Fig. 1. Hydrogen combustion engine market (US billion) [37]

Due to its geographical position, North America is expected to have a significant share in the market for hydrogen-powered internal combustion engines in the upcoming

timeframes. This is driven by increasing investments in research and development aimed at creating cutting-edge solutions and meeting end-user requirements. Additionally, U.S. government programs promoting eco-friendly energy sources are fostering market expansion across the region. Although hydrogen internal combustion engines are still in the early stages of development, policymakers are encouraged to support their adoption due to the adverse effects of CO_2 emissions in both industrialized and developing countries, such as the United States and China. The European government has called on manufacturers to reduce CO_2 emissions in new road vehicles by approximately 30% starting in 2030. Similar emission reduction targets have been set by the United States and China.

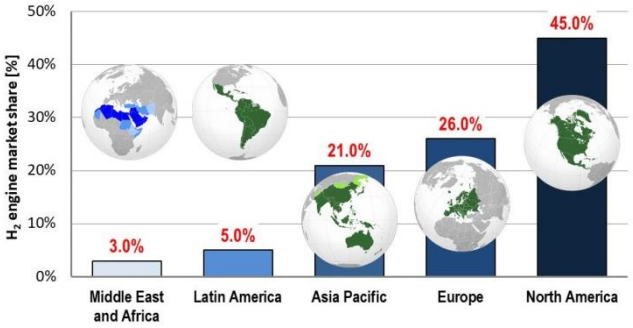

Fig. 2. Hydrogen combustion engine market share by region (in %) [37]

The hydrogen-powered internal combustion engine market is expected to experience the highest growth in the Asia-Pacific region during the forecast period (Fig. 2). This growth is driven by the expansion of key market players in the region and rising fuel prices, which will propel market development in the coming years.

Germany, the Netherlands, Poland, Italy, France, Spain, the United Kingdom, and Belgium are the eight largest hydrogen producers [45] in Europe (Fig. 3). These countries account for 74% of hydrogen produced through reforming processes, 83% of hydrogen generated as a by-product, 65% of hydrogen produced via water electrolysis, and nearly 100% of hydrogen produced through reforming combined with carbon capture.

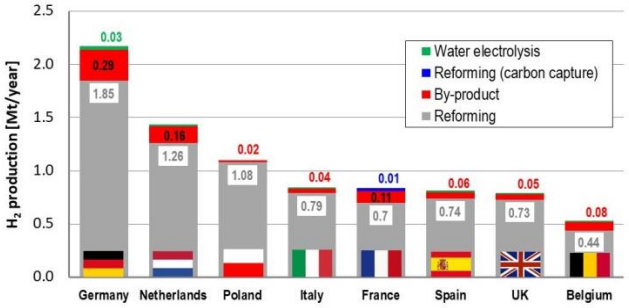

Fig. 3. Top 8 EU countries in terms of hydrogen production capacity by production process [45]

2. Hydrogen combustion engines

2.1. Hydrogen combustion with MPI and DI

The combustion of gaseous fuels (CH_4 and H_2) in internal combustion engines (SI and CI) primarily offers the potential to reduce the emissions of toxic exhaust components (Table 1). Moreover, these fuels can be relatively easily utilized in dual-fuel engine systems, significantly enhancing their potential for combustion or co-combustion. A comprehensive comparison of dual-fuel engines (powered by gasoline or diesel with hydrogen) was presented by Algayyim et al. [1]. Many examples pertain to typical CI engines and the addition of hydrogen up to 100%.

Table 1. Differences in the properties of low- and zero-emission fuels [2, 4, 9, 11, 13, 15, 22, 24, 30, 31, 47, 51]

Parameter	CNG	H_2 (Hydrogen)	Ethanol
Chemical composition and source	The dominant component is methane (CH_4)	The simplest element, produced by electrolysis, steam methane reforming, or biomass gasification	Ethyl alcohol, produced by fermentation of plants (corn, sugarcane)
Emissions and environmental impact	CO_2 emissions are about 53.1 kg/GJ, NO_x emissions are 90% lower than CI engines, and particulate emissions are 98% lower	No CO_2 emissions; emissions during hydrogen production depend on the method (e.g., electrolysis can be zero if renewable energy is used)	CO_2 emissions are about 70% lower than gasoline; NO_x emissions may be higher than gasoline
Calorific value	~50 MJ/kg	~120 MJ/kg	~27 MJ/kg
Efficiency in internal combustion engines	About 20–25% (like gasoline)	FC: about 50–60% ICE: about 30–40%	About 30–35%
Infrastructure cost	Relatively small	High (especially for storage and distribution)	Small (can be mixed with gasoline and use existing infrastructure)
Number of stations	Medium (developing)	Low (developing)	High (in countries with developed biofuel production)
Production cost	~4–5 USD/GJ	2–6 USD/kg (steam methane reforming), 4–5 USD/kg (electrolysis from renewable sources)	0.5–1 USD/dm^3 (biomass)
Operating cost	Relatively low due to lower fuel costs	High due to production and infrastructure costs	Higher than gasoline due to lower calorific value
Safety	Flammable gas under high pressure, requires appropriate tanks and safety systems	Highly flammable, stored under high pressure or cryogenically, requires special precautions	Less flammable than gasoline, but still requires appropriate safety measures
Research comparison of engines	Engines must be specially adapted for natural gas combustion	High material requirements for high temperatures and combustion control	Can operate on ethanol with minor modifications compared to gasoline engines
Combustion process simulation comparison	Indicates lower exhaust emissions compared to conventional CI and SI engines	High energy efficiency and no CO_2 emissions	Better efficiency than gasoline, but higher NO_x emissions

The laminar combustion speeds of methane and gasoline at $\lambda = 1$ obtain quite similar values (about 0.5 m/s) [6]. However, hydrogen under similar conditions achieves a laminar combustion rate approximately 10 times higher. The high flameability range, the very low ignition energy, and the high laminar flame speed make hydrogen produce a fast and short combustion event, fulfilling the requirements of an almost ideal combustion process – the isochoric combustion.

Direct injection of hydrogen increases the possibility of its combustion and at the same time increases the thermal efficiency of the process. Research by Wang et al. [49] indicate an efficiency value of 43.1% (in a turbocharged engine) with a compression ratio of approximately 14.5 (at $\lambda = 1.7$).

2.2. Fuel combustion in TJI

The two-stage combustion process increases the possibility of burning lean charges by using multi-point ignition and the possibility of effective ignition of the charge in the pre-chamber [56]. Positive results of methane combustion in an engine fueled with CH_4 are obtained in the range of lean fuel combustion (up to $\lambda = 2.2$) [35, 55, 58]. The combustion of CH_4 with hydrogen supplied to the pre-chamber causes the combustion of ultra-lean charges with $\lambda = 5.2$ [55] (Table 2).

Hydrogen combustion in engine systems concerns excess air coefficients ranging up to 2.0 (conventional system) [12, 32, 38] and up to 4 (with TJI system) [5, 34].

Ammonia is increasingly used in combustion engines (up to 0.1 m/s at $\lambda = 1.0$) [56]. The limitation of using only ammonia as a fuel is the very low laminar combustion rate. For this reason, dual-fuel systems are becoming more and more common in the TJI system.

There are many solutions for co-combustion of fuels using a two-stage combustion system (PC–MC): hydrogen-methane [26, 55]; hydrogen-ethanol [40, 41]; hydrogen-methanol [33]; hydrogen-diesel fuel [27, 28]; hydrogen-ammonia [17, 50 56, 57] or mixtures [18, 43]. All of them are based on the large flammability range of hydrogen and its high combustion rate, which ultimately leads to the combustion of lean or ultra-lean charges.

2.3. The influence of the geometry of the pre-chamber on fuel combustion

The pre-chamber, which is characterized by a specific volume, number and size of flow channels and their method of connection with the main chamber, has a significant impact on the initial quality of the combustion process (Table 2).

Aoyagi et al. [3], in experimental and simulation studies of CH_4 combustion, indicate that increasing the diameter of the holes reduces the flame outflow speed and, at the same time, increases the flame torch cone angle. Increasing the length/diameter ratio (L/D) also increases the discharge velocity but decreases the flame cone angle. An increase in the number of holes (with an almost unchanged flow surface area) indicates a limitation of the outflow speed with a large number of holes (10 pcs.). Despite such changes, the flame torch cone angle remained practically unchanged (the diameters were 4.0, 3.5, and 3.1 mm, respectively).

Research conducted by Jeelan Basha et al. [20] concerned the process of analyzing CH_4 combustion in RCM with a variable diameter of the single outlet hole of the pre-chamber (up to 1 to 4 mm). It was found that changes in the combustion process (at $\lambda = 2.5$) were observed only with a large hole diameter (4 mm), characterized by a limited combustion pressure. The highest HRR value was observed at d = 3 mm. Increasing the hole diameter resulted in a delay in the pressure increase after ignition. The analysis of flame angles indicates that they increase when the diameter of the holes increases (similar results were obtained in research [3]).

The use of different geometries of pre-chambers (6 variants) was analyzed in experimental engine tests [35] when powered by variable gas. It was found that multi-parameter optimization shows the best effects of using a pre-chamber containing both radial and radial holes (similar hole configurations were also studied in [14]). The research was carried out in terms of exhaust emissions and indicated engine efficiency with a variable fuel dose fed to the pre-chamber. The values of the excess air coefficient were in the range of $\lambda = 1.32–1.65$, at n = 1500 rpm and IMEP ~7 bar.

Simulation studies [25] on methane feeding in the range of changing the hole diameter (from 1.4 to 2.2 mm) indicate that the best solution in terms of combustion pressure and HRR is the value of 1.6 mm.

Guo et al. [14] found that during methane combustion, changing the diameter of the holes from 2.6 to 1.3 almost doubles the flow velocity of the torch (from 220 to 140 m/s) and increases the pressure difference in both chambers from 0.13 to 0.16 MPa.

The diameter of the discharge holes has less impact on the hydrogen combustion process. Research conducted by Liu et al. [26] indicates much greater differences in combustion pressure when using an active or passive chamber than when changing the hole diameter from 2 to 3 mm. When using a passive system, combustion at $\lambda = 3$ and higher causes a slow process. With an active system, this situation occurs only when $\lambda = 5$.

Motor research conducted by Tomić et al. [46] (when powered by gasoline) confirmed that the indicated efficiency data showed that a larger orifice area (OA) or larger orifice diameter at constant pre-chamber volume and orifice number is more favorable regarding the indicated efficiency.

The selection of the ammonia combustion chamber focuses on much smaller differences in the variants of the individual sizes of the pre-chamber. Research by Cui et al. [10] concerned changes in λ the range 1.0–1.4. The influence of the volume of the pre-chamber is significant in the range of lean loads (the greater the leanness, the more delayed combustion in a smaller volume, at a similar level of maximum pressure). Similarly to the combustion of methane, increasing the diameter of the holes when burning ammonia (from 2 to 3 mm) increases the range of the burning torches (by over 100%).

Simulation analysis of the angle of rotation of the discharge holes during gasoline combustion indicates that the degree of charge swirl is very important [16]. Straight channels do not show swirl, but turning the outflow by 30 degrees causes the swirl ratio to reach a value of 10. The tests showed that the highest HRR values were obtained when the holes were turned by an angle of 25 degrees, which resulted in SR = 8.

Table 2. Examples of solutions for the geometry of the initial combustion chamber (with the number of holes greater than 1)

No.	Reference	Volume PC [cm^3/% vol.]	No. × diameter	Fuel	Type of engine	Pre-chamber
1	Brunel University [7] (2019)	1.0/1.27% at TDC	6 × 1.25 mm	gasoline, Et	optical engine	active
2	University of Naples [5] (2024)	1.9/0,3%	6 × 1.15 mm	gasoline	simulation	active
3	University of Zagreb [46] (2023)	2.4/4.07% at TDC	6 × 1.30 mm	gasoline	engine	active
4	Marquette University [54] (2024)	2.0/1.94% at TDC	2 × 2.3 mm	E10-E90	simulation	active
5	Sandia National Laboratories [39] (2021)	4.66	8 × 1.6 mm (angle 130 deg)	Natural gas (95% CH_4)	optical engine	active
6	KAUST [44] (2021)	5.07/2.5% at TDC	2 row × 6 × 1.5 mm (angle 134 deg)	CH_4	optical engine	active
7	ETH [53] (2019)	1.0	4 × 1.2 mm (angle 120 deg)	CH_4	RCEM	passive
8	Shanghai Jiao Tong University [21] (2020)	–	6 × 2.9 mm	CH_4	CVC	active
9	PUT [35] (2019)	1.826/0.35% at TDC	7 × 1.5 mm (radial) + 3 × 1.4 mm (axial)	CH_4	engine	active
10	Kyushu University [3] (2024)	2.3%	10 × 3.1 mm	CH_4	CVC	passive
11	EMPA [43] (2020)	1.8/0.5% at TDC	7 × 1.5 mm	CH_4/HCH_4	engine	active/passive
12	Beijing Institute of Technology [52] (2018)	1.5	6 × 1.0 mm	H_2	CVC	active
13	PUT [36] (2024)	2.29/0.45% at TDC	6 × 1.5 mm	H_2	engine	passive
14	Shanghai Jiao Tong University [57] (2024)	–	6 × 1.4 mm (angle 140 deg)	H_2 (PC) NH_3 (MC)	simulation	active
15	Universidade Federal de Minas Gerais [40] (2019)	0.88/2.2% at TDC	4 × 1 mm (angle 45 deg) + 1 × 2 mm (axial)	H_2 (PC) Et (MC)	engine	active/passive

3. Purpose and scope of engine research work

The aim of the research is to determine the thermodynamics of the hydrogen combustion process, considering geometric changes in the flow channels and the variable fuel dose fed to the pre-chamber. Such control allows (1) to change the use of the pre-chamber from passive to active, (2) to change the thermodynamics of hydrogen combustion, (3) to change the amount of inter-chamber flows of the charge and to simultaneously change the fuel-air ratio in the pre-chamber. The size of the dose administered to the pre-chamber slightly changes the global value of the excess air coefficient, but significantly defines this value in the pre-chamber.

4. Research methodology

4.1. Research object

Simulation tests were carried out using AVL Fire 2022.1 software. A movable combustion chamber mesh was used (Fig. 4) with the parameters presented in Table 3. The mesh represents the combustion chamber of the cylinder with a displacement of 510.7 cm^3. The mesh consists of a pre-chamber, a main chamber, and outflow holes. The mesh is divided into sections that represent the elements of the moving mesh.

The authors used the combustion chamber without considering the engine's intake and exhaust channels due to the simplicity of the model and the implementation of direct fuel injection. This approach appears in many publications [19, 21, 29]. The conditions for starting the compression process correspond to the conditions of the research engine, so the representation of a typical combustion engine has been preserved.

Figure 5a shows the location of the injector. Due to the lack of engine intake and exhaust channels (the model considers only the closed space of the cylinder), fuel injection into the main chamber was carried out by placing the injector

Table 3. Combustion chamber and mesh parameters

Parameter	Unit	Value
S	mm	90
D	mm	85
V_{cyl} (TDC)	cm^3	557
V_{cyl} (BDC)	cm^3	47,2
V_{PC}	cm^3	1.61
Max number of cell (TDC)	–	32 k
Max number of cell (BDC)	–	138 k
Surface cell size (min)	mm	0.2

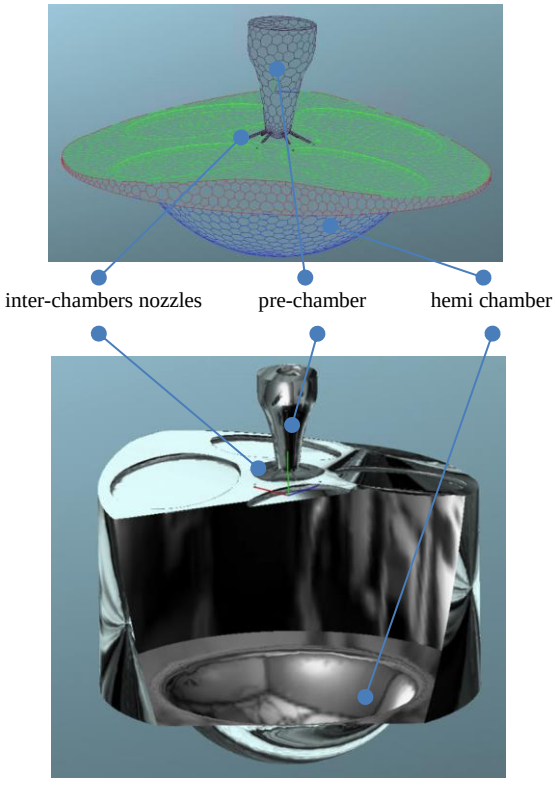

Fig. 4. View of the combustion chamber with elements marked

at an angle between the valves. Fuel was injected into the pre-chamber with a vertically placed injector next to the spark plug (Fig. 5b). This location of the injector may cause some of the gas to enter the main chamber. The angularly placed injector in the main chamber causes the gas to mix with the air, whose Turbulent Kinetic Energy (TKE) is initially 10 m^2/s^2. The fuel injection start time was set at 550 deg. The end of injection was simulated at an angle of 600 deg. An angular time of 50 deg was set for both combustion chambers, primary and main (at n = 1500 rpm, the injection duration is approximately 5.55 ms). The initial values enable fuel injection at low pressure (in the works [32, 36], such injection was carried out at a pressure of 3–7 bar). The ignition angle for all cases was set at 711 deg (9 deg bTDC). This ignition angle prevents the maximum combustion pressure from occurring too early and heat release around 5–10 deg aTDC.

a) b)

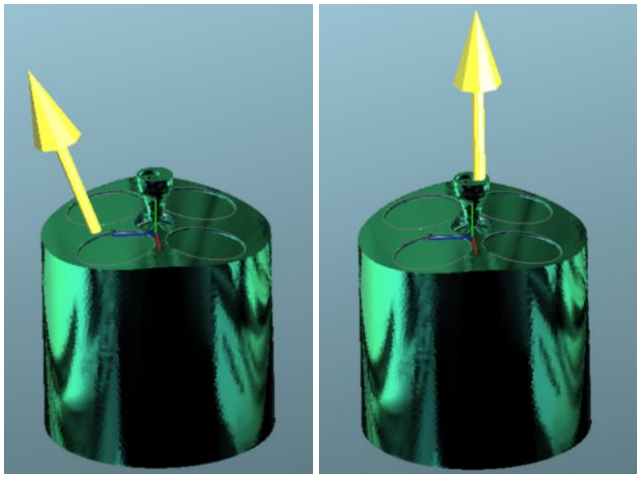

Fig. 5. View of the combustion chamber with the location of the injector marked: a) in the main chamber; b) in the pre-chamber

4.2. Research methodology

Combustion process tests were carried out in the range from 540 to 800 deg CA. It was assumed that the beginning of the cycle begins at an angle of 360 degrees. This is since it is possible to analyze the valve coverage from the previous calculation cycle. For this reason, TDC (hot) is at 720 deg. The boundary conditions are included in Table 4. These conditions apply to low boost pressure (which results from the assumed intake pressure value). It is sufficient to achieve a high charge depletion in the engine's main combustion chamber (MC).

Table 4. Boundary conditions

Parameter	Value
Pressure	100 000 Pa
Density	1.19 kg/m^3
Temperature	293.15 K
Turb. kin. energy (TKE)	0.001 m^2/s^2
Turb. length scale	0.001 m
Turb. diss. rate	0.00519616 m^2/s^3

The combustion process was analyzed using the models included in Table 5. A typical value of rotational speed was assumed (n = 1500 rpm). The combustion module in the form of the Turbulent Flame Speed Closure Model [23] was used. The essence of this model is the determination of the reaction rate based on an approach depending on parameters of turbulence, i.e., turbulence intensity and turbulent length scale, and of flame structure like the flame thickness and flame speed [23, 48].

Model k-epsilon usually yields reasonably realistic predictions of major mean-flow features in most situations. It is particularly recommended for a quick preliminary estimation of the flow field or in situations where modeling other physical phenomena, such as chemical reactions, combustion, radiation, and multi-phase interactions, brings uncertainties that outweigh those inherent in the k-ε turbulence model.

Table 5. Simulation parameters

Run mode	Crank angle
Start angle	540 deg
End angle	800 deg
Engine speed	1500 rpm
Min/max iteration	5/20
Module activation	Species transport
	Combustion (Turbulent Flame Speed Closure Model)
	Emission (Extended Zeldovich)
	Spray
Turbulence model	k-epsilon
Wall treatment	Hybrid Wall Treatment
Heat transfer wall model	Standard Wall Function

The tests were carried out according to a 3 × 3 matrix, including different diameters of the pre-chamber holes (0.5, 1.0, and 1.5 mm) along with different doses of fuel fed to the pre-chamber. Fuel doses with values 0, 0.4, and 1.2 mg were adopted to achieve combustion with a passive chamber (qo_PC = 0 mg) and an active chamber (qo_PC > 0 mg).

5. Analysis of the influence of geometry and fuel dose on the combustion process

5.1. Analysis of fast-varying processes

Cylinder pressure

Tests on the compression pressure and combustion of hydrogen were carried out in a closed combustion chamber (charge exchange was not analyzed). The modeled sections of the moving mesh allowed for the assessment of the pressure in the pre-chamber (PC) and main chamber (MC). Small holes in the pre-chamber (d = 0.5 mm – Fig. 3a) cause significant attenuation of the pressure in the pre-chamber. At the ignition angle (711 deg), the pressure values are 20.7 bar (PC) and 32.0 bar (MC), respectively. In this way, ΔP = 11.3 bar pressure difference is obtained. The significant difference in pressure in PC compared to MC causes the combustion process in PC to be very violent. This means that the charge is close to the stoichiometric charge. The smallest hole diameters cause the maximum pressure in the MC to be the lowest in all analyzed solutions. Despite this, the pressure in PC is higher than in MC and is achieved at a much larger angle. The difference is up to 5 deg (with a passive chamber – Fig. 6a). This means that the small flow holes significantly eliminate the flow of flames into the main chamber. They are probably also ex-

tinguished on the walls of the holes, which may reduce the pressure in the main chamber.

Large hole diameters mean that a larger part of the dose from the main chamber goes to the pre-chamber. This results in increased combustion pressures in the PC in the initial phase of the process.

This is the only case of such changes because increasing the diameter of the holes no longer causes such differences (Fig. 6b and 6c). Additionally, the combustion pressures overlap and are the same at the largest analyzed diameter. With hole diameters d = 1.0 and 1.5 mm, an increase in the combustion pressure in the PC is visible (a characteristic hump of the combustion process). The largest hole diameters result in the highest combustion pressures. This means that holes with a diameter of 1.0 mm and larger do not limit the flow of charge to the PC or the outflow of flames from the PC. Additionally, the flame does not go out, which increases the pressure in the main chamber. In relation to a large dose and large diameter, a characteristic increase in pressure in the PC is observed, indicating the violent nature of combustion (only in the case of the active chamber). Similar tests using alternating gas (d = 2.5; 3.0; 3.5 mm) [3] indicated a large range of burning torches for smaller hole diameters. However, these diameters were not the limit values for extinguishing the methane flame. In the work [46], it was found that increasing the diameter of the holes has a positive effect on the engine's IMEP.

Pre-chamber–main chamber flow characteristic

The magnitudes of the pressure difference in both chambers are shown in Fig. 7 When using holes with the smallest diameter (d = 0.5 mm), the largest pressure differences are observed in both chambers. The first signs of this are visible during fuel injection. This injection takes place in the range of 550–600 deg (in both chambers simultaneously). With minimal hole diameters, a significant pressure build-up in the PC is visible during injection (passive chamber). Increasing the dose to PC reduces the pressure difference (Fig. 7a). Increasing the diameter of the holes increases interchamber flows and at the same time reduces the pressure difference during fuel injection (Fig. 7b). With a diameter of d = 1.5 mm, the pressure difference is below 1 bar (Fig. 7c). Similar interchamber flow relationships are observed with diameters d = 1.0 and 1.5 mm. The course of the pressure difference curves is similar. The larger the holes, the smaller the pressure differences. It is worth noting that the largest differences concern the pressure moments after ignition. The greatest differences were noted at d = 1.5 mm and at a PC dose of 0.4 mg. This may mean that such a dose results in the best composition of the flammable mixture in the pre-chamber.

5.2. Analysis of average thermodynamic quantities

Temperature in the cylinder

The analysis of the temperature distribution in both combustion chambers is presented in Fig. 8. According to the large pressure differences at d = 0.5 mm, similar changes were recorded in terms of temperature changes. Fuel injection into the PC reduces the average temperature value before ignition. Using a passive chamber, 699°C was recorded in the PC before ignition. In the active chamber, this value decreased by over 60°C to 627–633°C. This means that when using small holes in the PC, throttling the flow not only limits the pressure in the main chamber but also greatly limits the temperature (Fig. 8a). No such tempera-

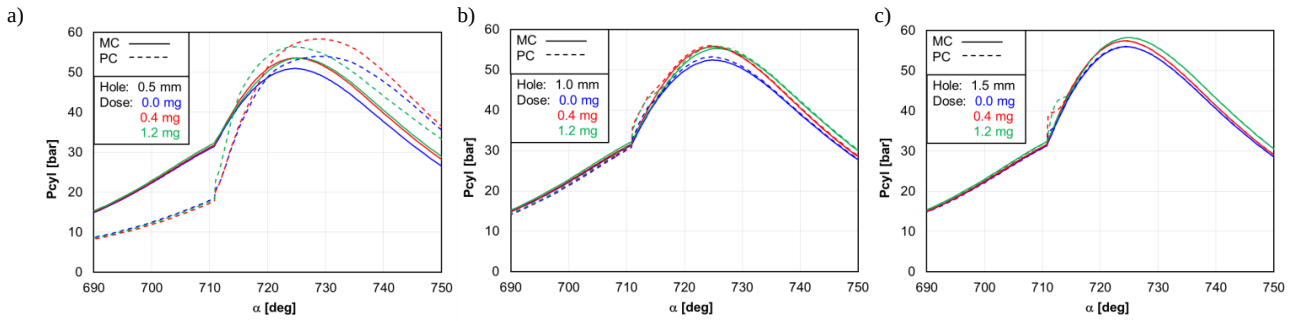

Fig. 6. Analysis of the pressure difference in the pre-chamber and main chamber with different configurations of the diameter of the outflow holes from the pre-chamber: a) 0.5 mm, b) 1.0 mm, c) 1.5 mm and different fuel doses

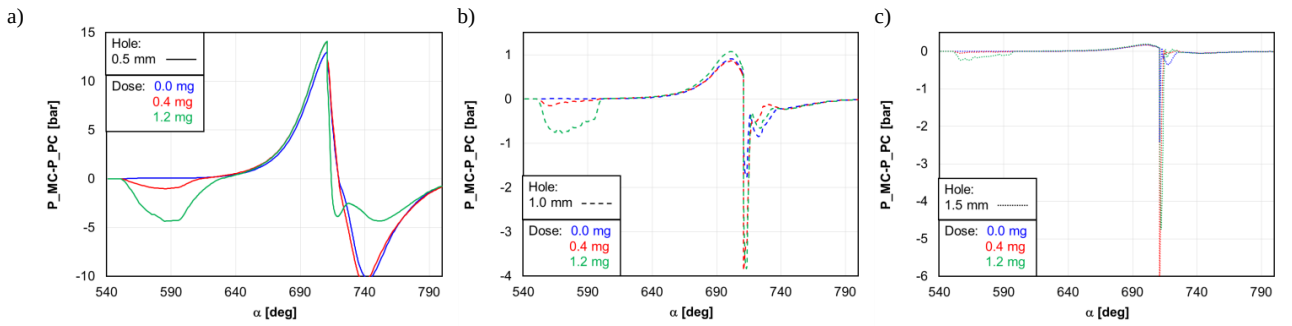

Fig. 7. Analysis of the pressure difference in the pre-chamber and main chamber with different configurations of the diameter of the outflow holes from the pre-chamber: a) 0.5 mm, b) 1.0 mm, c) 1.5 mm and different fuel doses

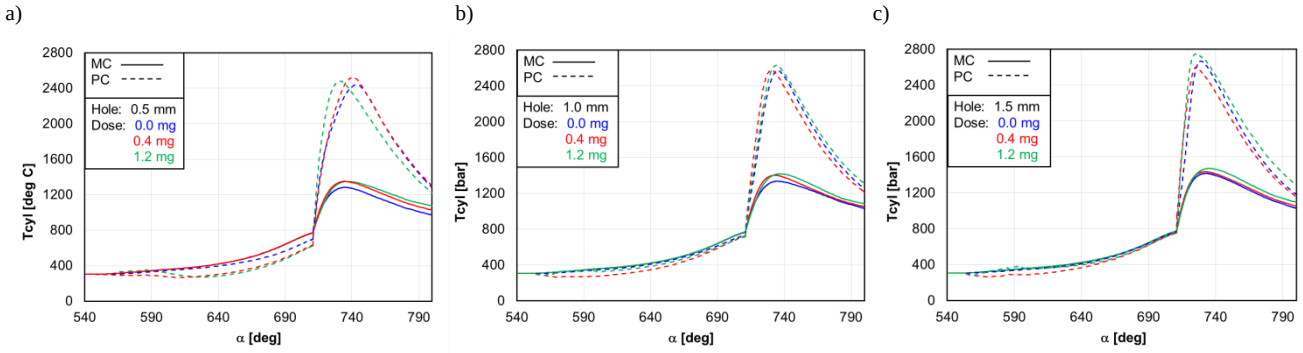

Fig. 8. Analysis of the temperature in the preliminary chamber (dashed line) and main chamber (solid line) with different configurations of the diameter of the outflow holes from the preliminary chamber: a) 0.5 mm, b) 1.0 mm, c) 1.5 mm and different fuel doses

ture changes were recorded for holes with a diameter of 1.0 and 1.5 mm. The differences are only due to fuel injection into the PC, which results in a slight temperature drop. However, until the moment of ignition, these values are equal (changes are below 3°C). As a result of the combustion process, which takes place in the pre-chamber at a much lower value of the excess air coefficient, much higher temperatures are observed. As the diameter of the holes increases, the maximum temperature values in the pre-chamber increase. This means increasing the uniformity of the charge in this chamber. There was also a slight but constant increase in the maximum temperature value in MC. This proves the greater dynamics of the flow of burning fuel flares (Fig. 8b and 8c).

Air-fuel ratio

The previously presented values also depend on the air-fuel ratio in both combustion chambers. The λ values in the pre-chamber are shown in Fig. 9a. The lack of fuel dose (qo_PC = 0 mg) results in significant differences in the formation of this value before ignition. Regardless of the diameter of the holes, the value of λ is approximately 0.4 units different (smaller) in the case of feeding the pre-chamber. Fuel injection into the PC causes λ to reach a value close to zero, which means that almost the entire chamber is filled with fuel. At the ignition angle (711 deg), the value of the excess air coefficient approaches the steady charge (the dose to PC was not previously selected, as a result of which λ = 1 was not obtained in the pre-chamber). The influence of the size of the holes and inter-chamber flows causes those changes in λ and the diameter of the holes do not have a fixed tendency. Analyzing data on Fig. 9a, it can be concluded that an almost stoichiometric charge was obtained at d = 1.0 and the highest dose of fuel to the pre-chamber (1.2 mg). In the absence of fuel fed to the PC, with the hole diameter d = 1.0 mm, the value of λ was also obtained close to the value of 1. Each other research case (regardless of the passive or active chamber caused the value of the excess air coefficient to be less than 1 (which meant the load rich in the pre-chamber). Injection of the fuel dose only into the main chamber resulted in a constant and fixed value of the excess air coefficient equal to 3.1 (regardless of the diameter of the holes (no PC participation in charge formation). With the pre-chamber active, a reduction in the excess air coefficient is observed to 2.9 and 2.6, respectively (Fig. 9b).

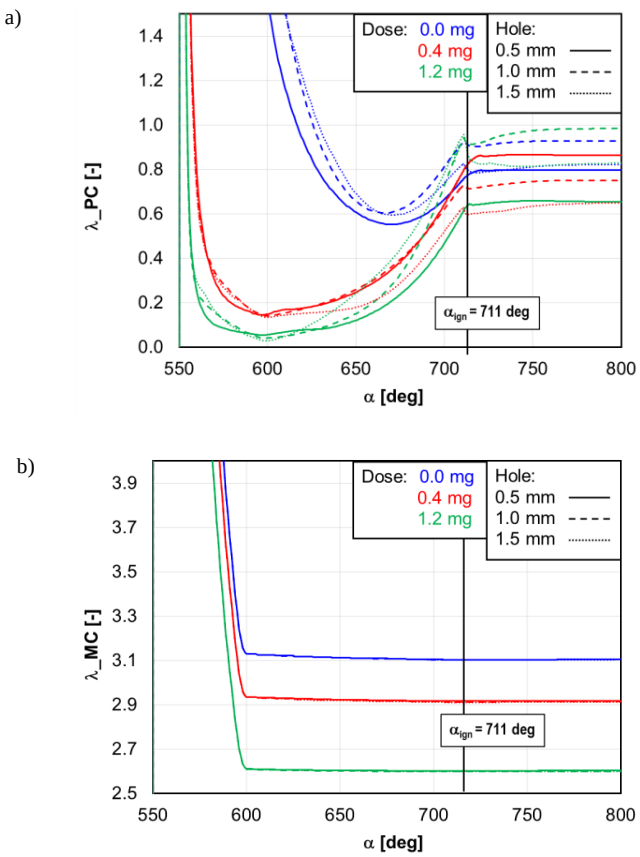

Fig. 9. Analysis of the excess air coefficient in the pre-chamber λ_PC (a) and in main chamber λ_MC (b) with different configurations of the diameter of the outflow holes from the pre-chamber and different fuel doses

As can be seen from the graphs in Fig. 6a, the diameter of the holes is significantly more important than the dose size in creating the final value of the excess air coefficient in the vicinity of the ignition angle. There is no clear relationship between the value of λ and the fuel dose and the diameter of the holes. With a high fuel dose, the lowest λ values were obtained with the average diameter of the holes, and with a dose of 0.4 mg – with the lowest λ. It follows that interventricular flows play an important role in the final value of λ in PC.

Heat release

The amount of released heat was considered separately in the preliminary and main chambers. Passive chambers (qo_PC = 0) with small hole diameters were characterized by a limited heat release rate, which results from the relatively slow growth of the curves (Fig. 10a). The largest amount of heat released in the PC (for a passive chamber) occurs at d = 0.5 mm and a dose of 0.4 mg. The highest Q value for all test cases was obtained with the highest dose to PC and the largest hole diameter. Increasing the dose to PC increases the maximum amount of heat released in this chamber. The decrease in heat in the PC is due to the flow of charge (and heat) into the main chamber. The combustion process in the pre-chamber is partially correlated with the heat release in the main chamber (Fig. 10b). The lowest amount of heat was recorded at d = 0.5 mm and the passive chamber. The highest amounts of heat were recorded with a large dose of fuel for the PC and a large diameter of the holes.

The combustion of fuel in the main chamber causes the amount of heat to increase with the dose to PC. The highest combustion rates in the MC were recorded with a large dose of fuel fed to the PC.

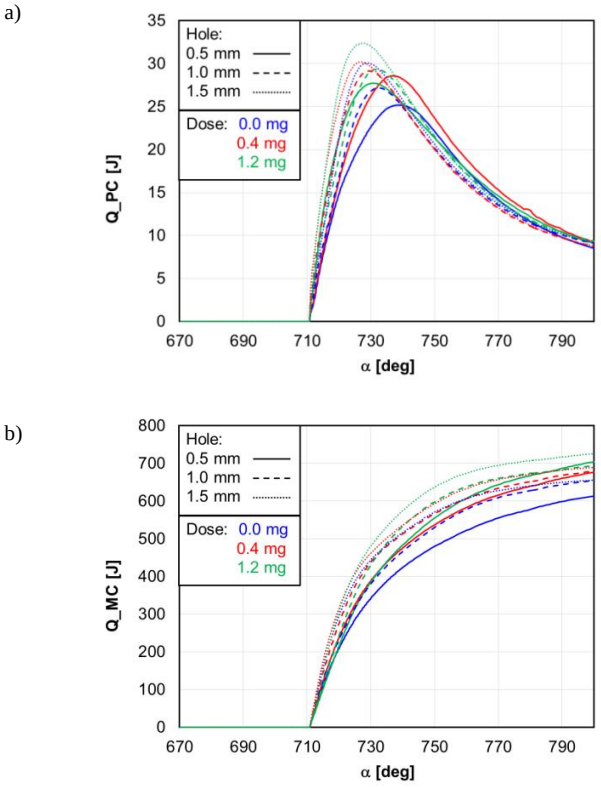

Fig. 10. Analysis of the amount of heat release in the pre-chamber Q_PC (a) and in main chamber Q_MC (b) with different configurations of the diameter of the outflow holes from the pre-chamber and different fuel doses

The increase in the amount of heat when increasing the dose to PC indicates an improvement in the combustion quality in MC and PC. Improving the combustion quality in PC also results in better combustion in MC. This is due to the fact that increasing the dose by 1.2 mg causes a maximum heat to increase of 144 J. The analysis of the best and worst course in Fig. 7b indicates differences of just over 100 J. Large analogies are also observed in the same waveforms in the pre-chamber (the same waveforms reach extremely different values).

NO formation

The amount of nitrogen oxides produced is closely related to the combustion conditions. Even though the maximum temperatures in PC are over 1000 K higher than in MC, the amount of NO produced is an order of magnitude lower than in MC (Fig. 11a and 11b). This is due to the duration of combustion in each chamber. Shorter combustion time in PC generates lower NO values. The lowest amounts of NO were recorded when the engine was powered by passive chambers. The molar fractions of NO in the pre-chamber are closely related to the dose size and the diameter of the holes (the larger the doses and hole diameters, the more NO). Regarding NO production, the diameter of the holes is more important than the amount of fuel dose fed to the PC (the highest initial intensity of NO formation is at large hole diameters). When analyzing the PC and MC chambers, a higher amount of NO was recorded in the main chamber (the difference is exactly 1 order of magnitude: 0.002 and 0.0002, respectively).

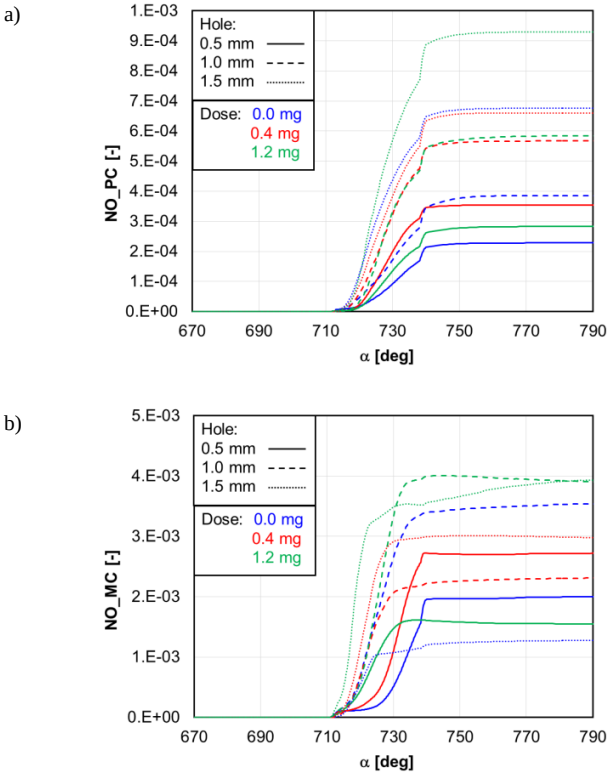

Fig. 11. Analysis of NO in the pre-chamber NO_PC (a) and in main chamber NO_MC (b) with different configurations of the diameter of the outlet holes from the pre-chamber and different fuel doses

5.3. Analysis of thermodynamic quantity distributions

The average values of thermodynamic indicators are now compared with instantaneous values. Hydrogen injection into the main chamber was simulated as direct injection. This has a large impact on the form of the created charge. Analysis of the distribution of the air-fuel ratio (Fig. 12) indicates a significant lack of uniformity of the load.

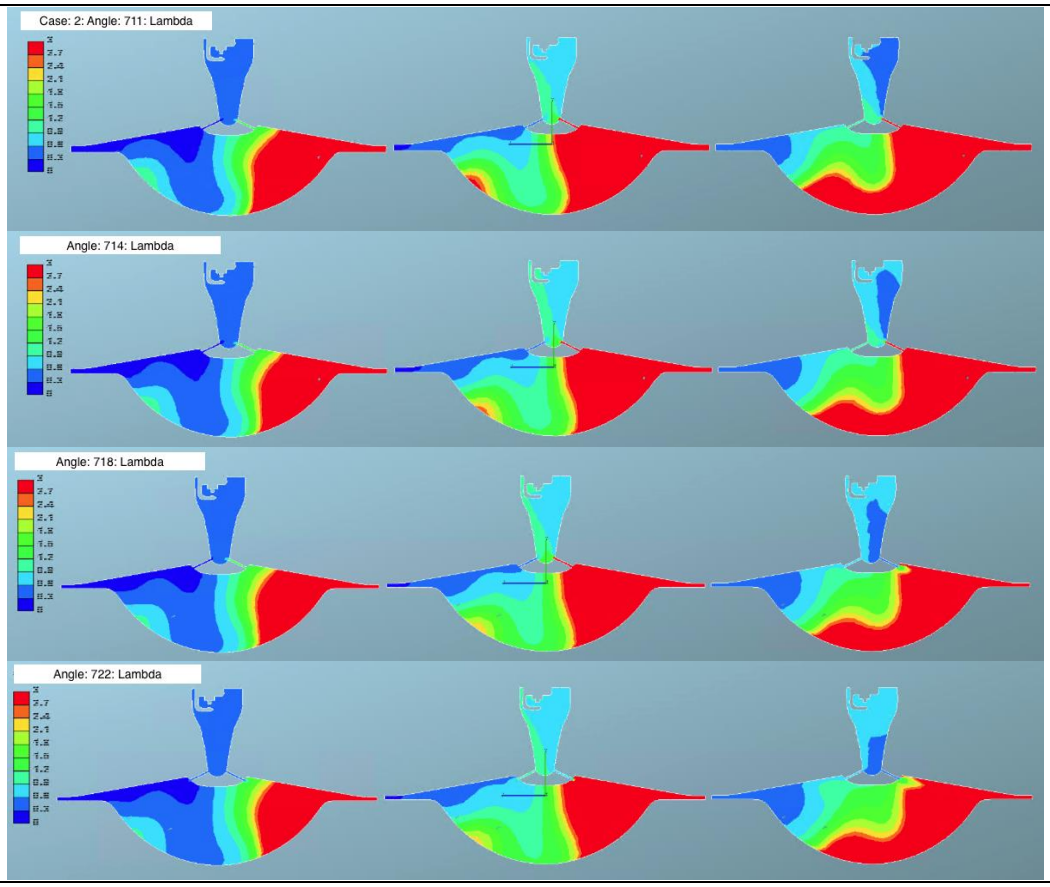

Fig. 12. Analysis of the distribution of the excess air coefficient in the pre-chamber λ_PC and main λ_MC with various configurations of the outflow hole diameter and a constant value of qo_PC = 0.4 mg

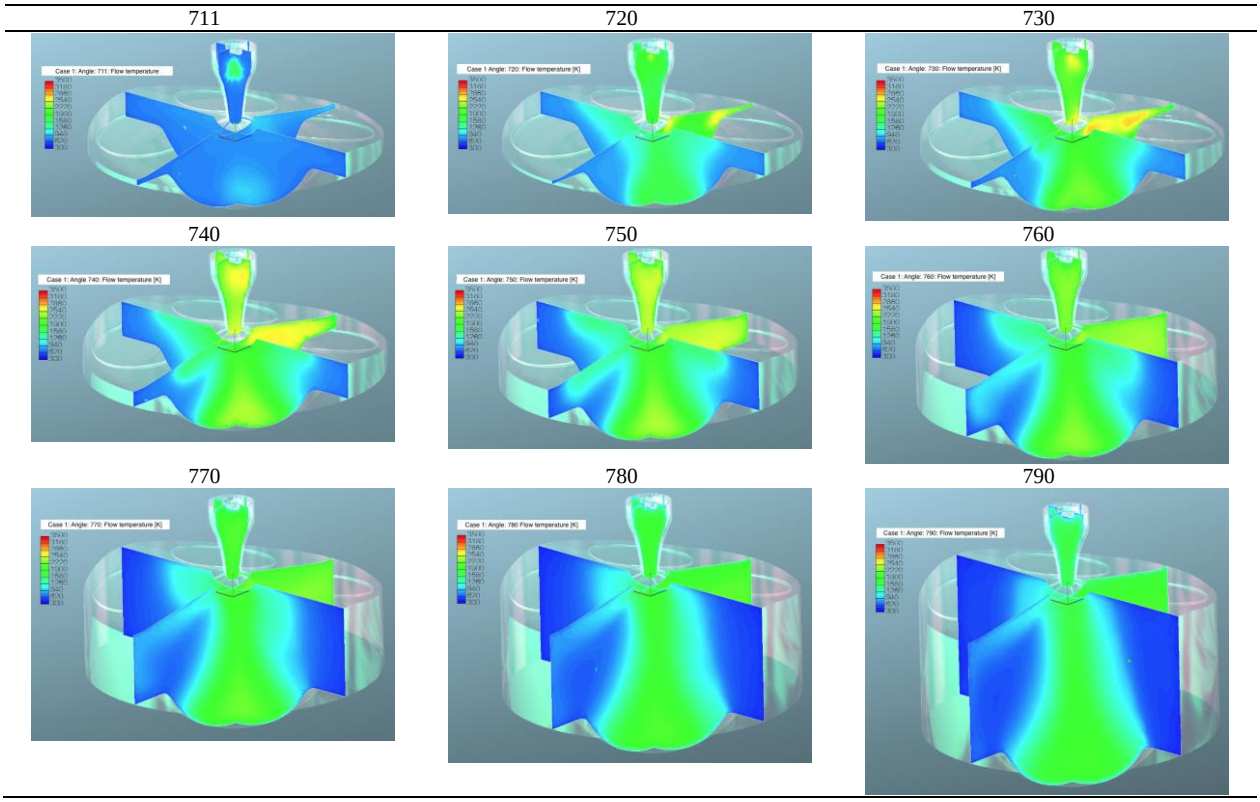

Fig. 13. Analysis of the temperature distribution in the preliminary chamber λ_PC and main λ_MC at d = 0.5 mm and qo_PC = 0 mg (passive chamber)

Due to the injection method (Fig. 5), a characteristic division of the MC chamber into two zones, rich and lean in fuel, was achieved. A similar relationship is observed in the pre-chamber. With a small hole diameter, the tendency of division and zones is dominant in the main chamber, and as the diameter of the holes increases, the division in the main chamber decreases and it increases in the pre-chamber.

Due to the uneven charge formation in both chambers, the combustion temperature distribution is also not the same (Fig. 13). At an angle of 740 deg, the maximum temperature is observed in the PC and MC chambers. These results are consistent with the data presented in Fig. 8, which concerned average values.

The analysis of the temperature distribution with the same dose to the PC (qo = 0.4 ms) is presented in Fig. 14. It shows that the large diameter of the holes facilitates the flow of charge into the PC, causing an increase in the temperature value in a small volume during ignition. The high temperature remains up to 720°C. Despite the large diameter of the holes and the average dose value, a large variation in the charge distribution in the main chamber is observed.

5.4. Maps of thermodynamic quantities

The solutions presented above regarding the analysis of average and instantaneous engine operation indicators enabled the construction of detailed maps. These maps were created in coordinates: hole diameter–fuel dose. Their structure makes it possible to initially determine the tendency of changes in engine operating indicators when one or another parameter is changed.

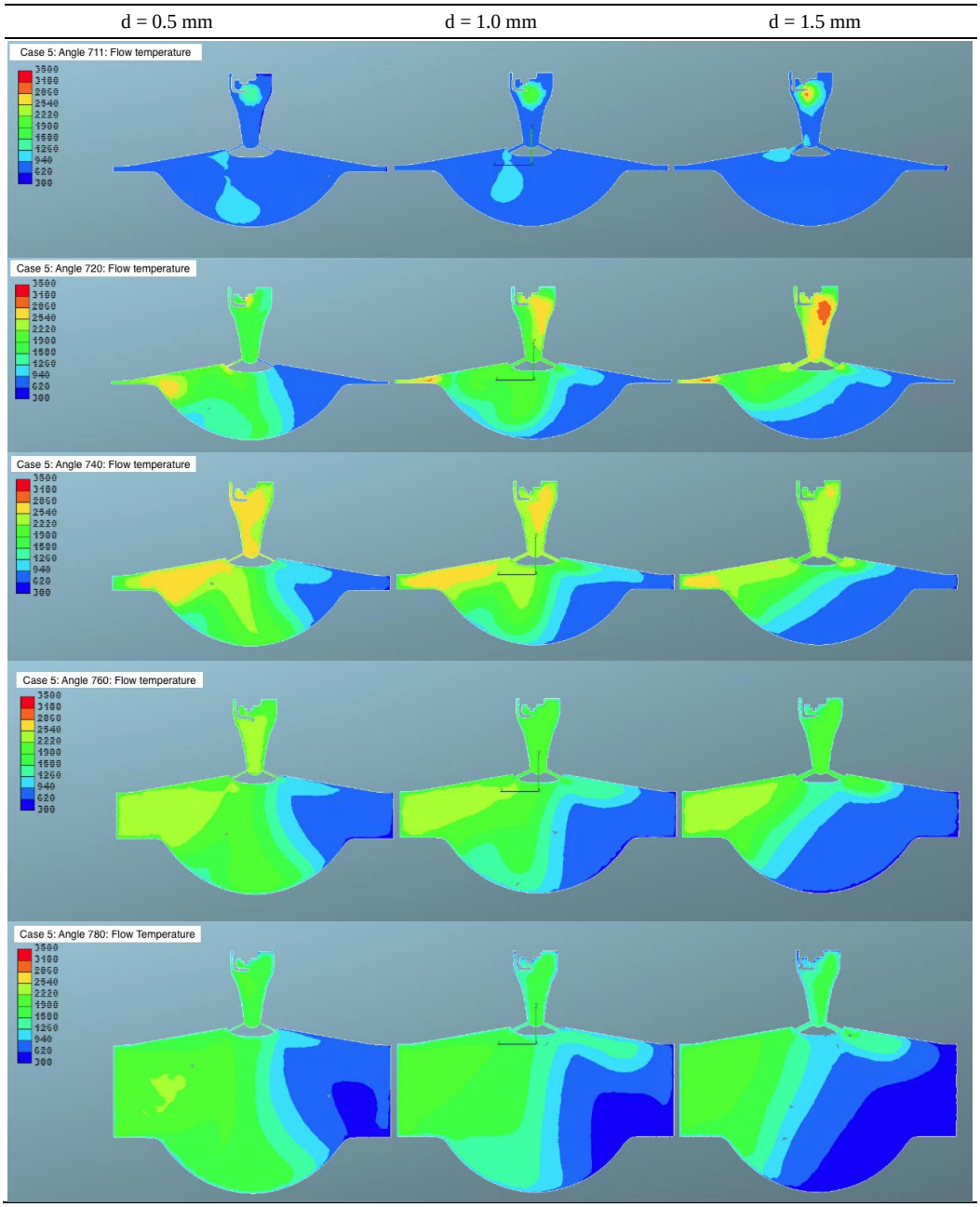

Fig. 14. Analysis of the charge temperature distribution in the cylinder with various hole diameter configurations and a constant fuel dose to the pre-chamber qo_PC = 0.4 mg

The analysis of the pressure distribution in the cylinder in both chambers (Fig. 15) only partially correlates with the amount of released heat. In the pre-chamber, these values are consistent only in the range of large doses to PC and large hole diameters. In the remaining parts of the map, small and medium doses and small hole diameters do not show any correlation. When comparing the main chamber, the correlations are even smaller; this may result primarily from the lack of uniformity of the created charge.

Similar conclusions were obtained when analyzing temperature and NO in both chambers (Fig. 16). In the pre-chamber, a high correlation of temperature and NO formation was obtained in all areas of the d–qo_PC map. The highest NO formation was recorded where the highest temperature was also observed. Unfortunately, this tendency does not occur in the case of the main compartment. As before, it may result from large charge heterogeneity. It follows that fuel injection directly into the cylinder should

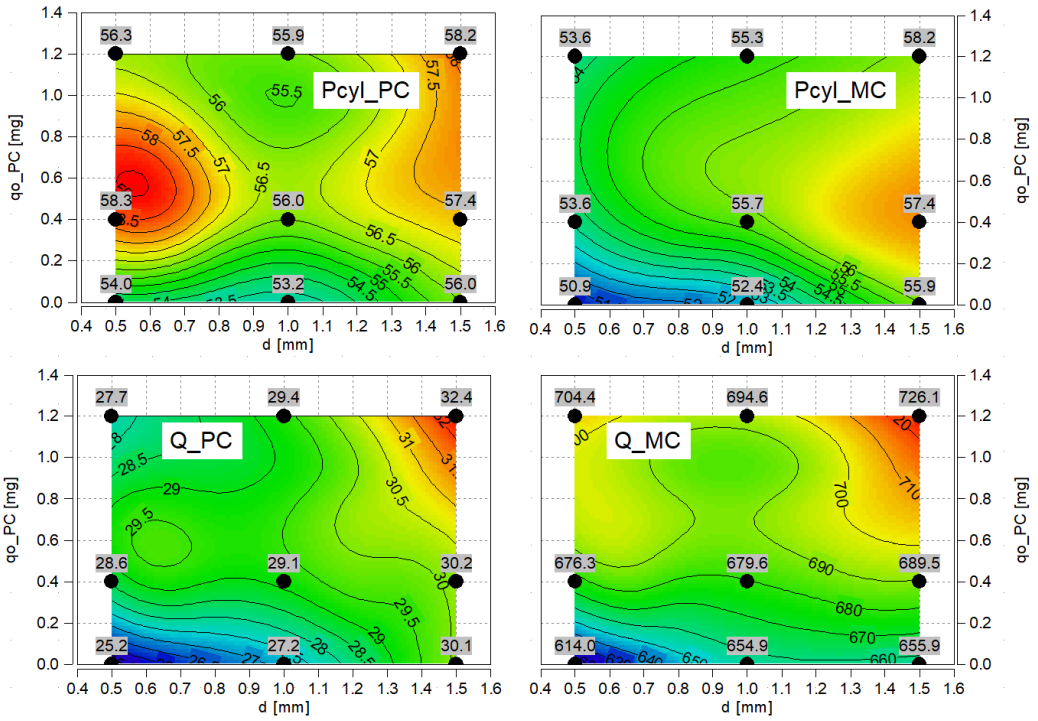

Fig. 15. Map of pressure changes in the cylinder and the amount of heat released in d–qo_PC coordinates: a) in the pre-chamber, b) in the main chamber

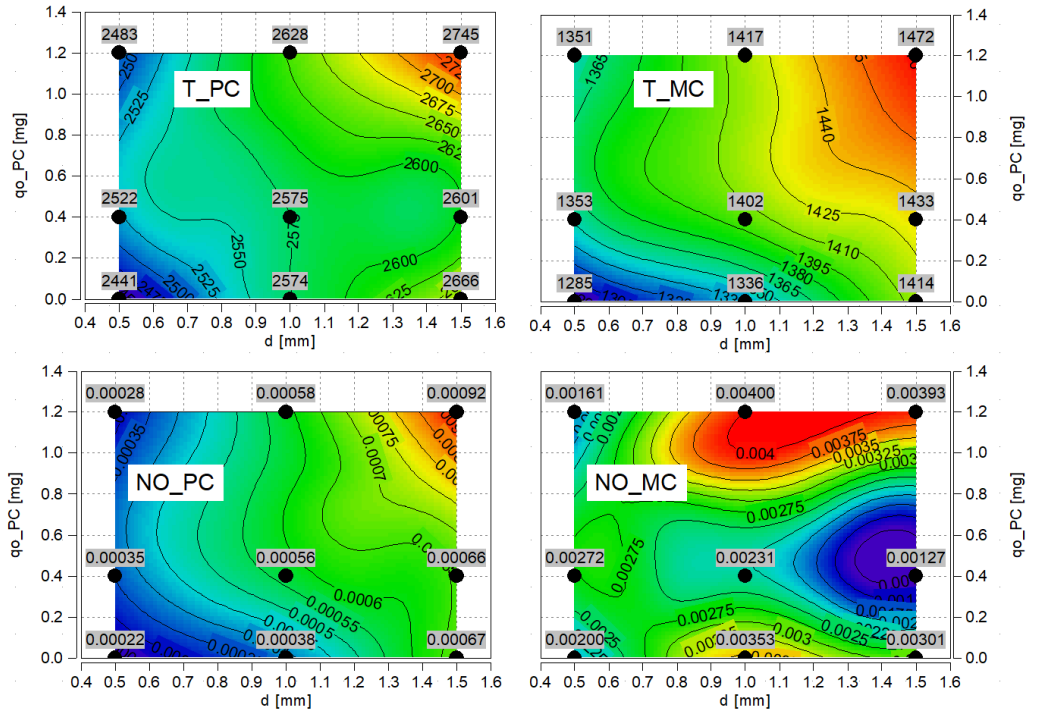

Fig. 16. Map of temperature changes in the cylinder and the amount of NO in d–qo_PC coordinates: a) in the pre-chamber, b) in the main chamber

be performed with a higher injection advance (than 550 deg) or injection should be used with a higher fuel pressure (increasing the range of the gas stream and its atomization in the main chamber). Another possibility may be a different location of the injector or division of the injected fuel dose.

6. Summary

Changing the diameters of the discharge holes significantly changes the combustion process in the TJI engine. Small hole diameters d ≤ 0.5 mm limit the flow of charge into the PC, which results in much lower pressures in the PC. Additionally, the outflow of the flame torches causes their extinction on the channel walls, which results in lower ignitability of the charge in the main chamber. It follows that the quenching distance of 0.6 mm given in the literature is effective [8, 42].

Based on the research work carried out, it was found that:

1. In terms of hole geometry:
   - too small sizes of flow holes (d ≤ 0.5 mm) cause significant throttling of the charge flow into the pre-chamber, which results in large differences in combustion pressure and, consequently, deterioration of the quality of the hydrogen combustion process
   - large diameters of flow holes (d ≥ 1.0 mm) minimize inter-chamber flow conditions, which results in no throttling and higher combustion rates (P_{cyl}, T_{cyl} and Q).
2. In terms of fuel consumption rates:
   - the diameter of the holes is much more important for the proper combustion process than the size of the fuel dose (outside the passive chamber)
   - in the conducted tests in the pre-chamber, an excess air-ratio fuel value close to 1 was obtained in the dose range qo_PC = 0.4 mg
   - increasing the diameter of the holes led to an increase in the maximum pressure in the cylinder and the rate of heat release. The highest values of pressure and heat release were observed with hole diameter d = 1.2 mm
   - the maximum temperature value in the cylinder increased with the increase in the diameter of the holes, which indicates an increase in the importance of inter-chamber flows
   - analysis of the distribution of the excess air-fuel ratio indicates a significant lack of uniformity of the load; Due to the method of fuel injection, a characteristic division of the MC chamber into two zones: rich and lean in fuel, was achieved
   - with a small diameter of the holes, the tendency to divide the zones is dominant in the main chamber, and as the diameter of the holes increases, the division into different spheres in the main chamber decreases, and the disproportion in the pre-chamber increases.

These conclusions constitute a solid basis for further research and experimental work, which may contribute to the development of more effective and ecological drive technologies. Subsequent research stages may be focused on the following issues:

- further optimization of hole diameters and fuel doses in order to determine the best relationship between hydrogen combustion efficiency and nitrogen oxide emissions
- experimental verification to confirm the quality of the simulation work carried out; subsequent work will allow for the calibration of models and a better understanding of the phenomena occurring during hydrogen combustion
- hydrogen injection with other fuels (e.g. NH_3) to increase combustion efficiency.

Nomenclature

BDC	bottom dead center
CFD	computational fluid dynamics
CVC	constant volume chamber
cyl	cylinder
d	diameter
DI	direct injection
dQ	heat release rate
LDV	light duty vehicle
MC	main chamber
MPI	multi point injection
NO	nitrogen oxide
P	pressure
PC	pre-chamber
qo	fuel dose
Q	heat release
RCEM	rapid compression expansion machine
SI	spark ignition
T	temperature
TDC	top dead center
TJI	Turbulent Jet Ignition
TKE	turbulent kinetic energy
λ	air excess ratio

Bibliography

[1] Algayyim SJM, Saleh K, Wandel AP, Fattah IMR, Yusaf T, Alrazen HA. Influence of natural gas and hydrogen properties on internal combustion engine performance, combustion, and emissions: a review. Fuel. 2024;362:130844. https://doi.org/10.1016/j.fuel.2023.130844

[2] Alleman TL, McCormick RL, Yanowitz J. Properties of ethanol fuel blends made with natural gasoline. Energy Fuels. 2015;29(8):5095-5102. https://doi.org/10.1021/acs.energyfuels.5b00818

[3] Aoyagi T, Wakasugi T, Tsuru D, Tashima H. Analysis of effects of pre-chamber orifices on torch flame behaviours in lean-burn gas engines. Combust Engines. 2024;199(4):3-14. https://doi.org/10.19206/CE-188112

[4] Barabás I, Todoruţ AI. Key fuel properties of bio-diesel-diesel fuel-ethanol blends. SAE Technical Paper 2009-01-1810. 2009. https://doi.org/10.4271/2009-01-1810

[5] Bozza F, Teodosio L, Krajnović J, Sjerić M, De Bellis V, Malfi E. Extensive validation of a combustion and pollutant

emission model of a pre-chamber engine including different pre-chamber geometries. Fuel. 2024;373:132282. https://doi.org/10.1016/j.fuel.2024.132282

[6] Bucherer S, Rothe P, Sobek F, Gottwald T, Kraljevic I, Vacca A et al. Experimental and numerical investigation of spark plug and passive pre-chamber ignition on a single-cylinder engine with hydrogen port fuel injection for lean operations. SAE Technical Paper 2023-01-1205. 2023. https://doi.org/10.4271/2023-01-1205

[7] Bureshaid K, Shimura R, Feng D, Zhao H, Bunce M. Experimental studies of the effect of ethanol auxiliary fueled turbulent jet ignition in an optical engine. SAE Int J Engines. 2019;12(4):387-399. https://doi.org/10.4271/03-12-04-0026

[8] Butler MS, Moran CW, Sunderland PB, Axelbaum RL. Limits for hydrogen leaks that can support stable flames. Int J Hydrog Energy. 2009;34(12):5174-5182. https://doi.org/10.1016/j.ijhydene.2009.04.012

[9] Crabtree GW, Dresselhaus MS. The hydrogen fuel alternative. MRS Bull. 2008;33(4):421-428. https://doi.org/10.1557/mrs2008.84

[10] Cui Z, Tian J, Zhang X, Yin S, Long W, Song H. Experimental study of the effects of pre-chamber geometry on the combustion characteristics of an ammonia/air pre-mixture ignited by a jet flame. Processes. 2022;10(10):2102. https://doi.org/10.3390/pr10102102

[11] Demirbas A. Fuel properties of hydrogen, liquefied petroleum gas (LPG), and compressed natural gas (CNG) for transportation. Energy Sources. 2002;24(7):601-610. https://doi.org/10.1080/00908312.2002.11877434

[12] Duan Y-h, Sun B-g, Li Q, Wu X-s, Hu T-g, Luo Q-h. Combustion characteristics of a turbocharged direct-injection hydrogen engine. Energy Convers Manag. 2023;291:117267. https://doi.org/10.1016/j.enconman.2023.117267

[13] Fayaz H, Saidur R, Razali N, Anuar FS, Saleman AR, Islam MR. An overview of hydrogen as a vehicle fuel. Renew Sustain Energy Rev. 2012;16(8):5511-5528. https://doi.org/10.1016/j.rser.2012.06.012

[14] Guo X, Li T, Chen R, Huang S, Zhou X, Wang N et al. Effects of the nozzle design parameters on turbulent jet development of active pre-chamber. Energy. 2024;306: 132568. https://doi.org/10.1016/j.energy.2024.132568

[15] Hansen A. Ethanol-diesel fuel blends – a review. Bioresour Technol. 2005;96(3):277-285. https://doi.org/10.1016/j.biortech.2004.04.007

[16] Hu J, Pei Y, An Y, Zhao D, Zhang Z, Sun J et al. Study of active pre-chamber jet flames based on the synergy of airflow with different nozzle swirl angle. Energy. 2023;282: 128198. https://doi.org/10.1016/j.energy.2023.128198

[17] Huo J, Zhao T, Lin H, Li J, Zhang W, Huang Z et al. Study on lean combustion of ammonia-hydrogen mixtures in a pre-chamber engine. Fuel. 2024;361:130773. https://doi.org/10.1016/j.fuel.2023.130773

[18] Ingo C, Tuuf J, Björklund-Sänkiaho M. Experimental study of the performance of a SI-engine fueled with hydrogen-natural gas mixtures. Int J Hydrog Energy. 2024;63:1036-1043. https://doi.org/10.1016/j.ijhydene.2024.03.252

[19] Jamrozik A, Tutak W, Kociszewski A, Sosnowski M. Numerical simulation of two-stage combustion in SI engine with prechamber. Appl Math Model. 2013;37(5):2961-2982. https://doi.org/10.1016/j.apm.2012.07.040

[20] Jeelan Basha KB, Balasubramani S, Sivasankaralingam V. Effect of pre-chamber geometrical parameters and operating conditions on the combustion characteristics of the hydrogen-air mixtures in a pre-chamber spark ignition system. Int J Hydrog Energy. 2023;48(65):25593-25608. https://doi.org/10.1016/j.ijhydene.2023.03.308

[21] Ju D, Huang Z, Li X, Zhang T, Cai W. Comparison of open chamber and pre-chamber ignition of methane/air mixtures in a large bore constant volume chamber: effect of excess air ratio and pre-mixed pressure. Appl Energy. 2020;260: 114319. https://doi.org/10.1016/j.apenergy.2019.114319

[22] Khan MI, Yasmin T, Shakoor A. Technical overview of compressed natural gas (CNG) as a transportation fuel. Renew Sustain Energy Rev. 2015;51:785-797. https://doi.org/10.1016/j.rser.2015.06.053

[23] Kido H, Nakahara M, Hashimoto J. A turbulent burning velocity model taking account of the preferential diffusion effect. In The 4th International Symposium COMODIA; 1998. https://www.jsme.or.jp/esd/laboratory/publishing/comodia/comodia1998/

[24] Li D, Zhen H, Xingcai L, Wu-gao Z, Jian-guang Y. Physico-chemical properties of ethanol–diesel blend fuel and its effect on performance and emissions of diesel engines. Renew Energy. 2005;30(6):967-976. https://doi.org/10.1016/j.renene.2004.07.010

[25] Li J, Wang Y, Xing K, Guo X, Chen K, Huang H. The influence mechanism of pre-combustion chamber orifice structure on natural gas engines: combustion, emissions, and thermofluid analysis. Appl Therm Eng. 2024;236:121654. https://doi.org/10.1016/j.applthermaleng.2023.121654

[26] Liu P, Zhong L, Zhou L, Wei H. The ignition characteristics of the pre-chamber turbulent jet ignition of the hydrogen and methane based on different orifices. Int J Hydrog Energy. 2021;46(74):37083-37097. https://doi.org/10.1016/j.ijhydene.2021.08.201

[27] Liu X, Aljabri H, Panthi N, AlRamadan AS, Cenker E, Alshammari AT et al. Computational study of hydrogen engine combustion strategies: dual-fuel compression ignition with port- and direct-injection, pre-chamber combustion, and spark-ignition. Fuel. 2023;350:128801. https://doi.org/10.1016/j.fuel.2023.128801

[28] Liu X, Aljabri H, Silva M, AlRamadan AS, Ben Houidi M, Cenker E et al. Hydrogen pre-chamber combustion at lean-burn conditions on a heavy-duty diesel engine: a computational study. Fuel. 2023;335:127042. https://doi.org/10.1016/j.fuel.2022.127042

[29] Lu Y, Qian Y, Zhang D, Chen Y, Pei Y. Parameters optimization of prechamber jet disturbance combustion system – effect of prechamber volume and fuel injection mass ratios on performance and exhausts in a diesel engine. Fuel. 2024; 373:132360. https://doi.org/10.1016/j.fuel.2024.132360

[30] Molnarne M, Schroeder V. Hazardous properties of hydrogen and hydrogen containing fuel gases. Process Saf Environ Prot. 2019;130:1-5. https://doi.org/10.1016/j.psep.2019.07.012

[31] Momirlan M, Veziroglu T. The properties of hydrogen as fuel tomorrow in sustainable energy system for a cleaner planet. Int J Hydrog Energy. 2005;30(7):795-802. https://doi.org/10.1016/j.ijhydene.2004.10.011

[32] Musy F, Ortiz R, Ortiz I, Ortiz A. Hydrogen-fuelled internal combustion engines: direct injection versus port-fuel injection. Int J Hydrog Energy. 2024; https://doi.org/10.1016/j.ijhydene.2024.07.136

[33] Palombi L, Sharma P, Cenker E, Magnotti G. Effects of engine speed on prechamber-assisted combustion. SAE Technical Paper 2023-24-0020. 2023. https://doi.org/10.4271/2023-24-0020

[34] Peters N, Bunce M. Active pre-chamber as a technology for addressing fuel slip and its associated challenges to lambda estimation in hydrogen ICEs. SAE Technical Paper 2023-32-0041. 2023. https://doi.org/2023-32-0041

[35] Pielecha I, Bueschke W, Skowron M, Fiedkiewicz Ł, Szwajca F, Cieślik W et al. Prechamber optimal selection for a two stage turbulent jet ignition type combustion system in CNG-fuelled engine. Combust Engines. 2019;176(1):16-26. https://doi.org/10.19206/CE-2019-103
[36] Pielecha I, Szwajca F, Skobiej K. Experimental investigation on knock characteristics from pre-chamber gas engine fueled by hydrogen. Energies. 2024;17(4):937. https://doi.org/10.3390/en17040937
[37] Precedence Research. Hydrogen Combustion Engine Market Size, Share, and Trends 2024 to 2034. 2023; https://www.precedenceresearch.com/hydrogen-combustion-engine-market
[38] Qiang Y, Ji C, Wang S, Xin G, Hong C, Wang Z et al. Study on the effect of variable valve timing and spark timing on the performance of the hydrogen-fueled engine with passive pre-chamber ignition under partial load conditions. Energy Convers Manag. 2024;302:118104. https://doi.org/10.1016/j.enconman.2024.118104
[39] Rajasegar R, Niki Y, García-Oliver JM, Li Z, Musculus MPB. Fundamental insights on ignition and combustion of natural gas in an active fueled pre-chamber spark-ignition system. Combust Flame. 2021;232:111561. https://doi.org/10.1016/j.combustflame.2021.111561
[40] Santos NDSA, Alvarez CEC, Roso VR, Baeta JGC, Valle RM. Combustion analysis of a SI engine with stratified and homogeneous pre-chamber ignition system using ethanol and hydrogen. Appl Therm Eng. 2019;160:113985. https://doi.org/10.1016/j.applthermaleng.2019.113985
[41] Santos NDSA, Alvarez CEC, Roso VR, Baeta JGC, Valle RM. Lambda load control in spark ignition engines, a new application of prechamber ignition systems. Energy Convers Manag. 2021;236:114018. https://doi.org/10.1016/j.enconman.2021.114018
[42] Saravanan N, Nagarajan G, Sanjay G, Dhanasekaran C, Kalaiselvan KM. Combustion analysis on a DI diesel engine with hydrogen in dual fuel mode. Fuel. 2008;87(17-18): 3591-3599. https://doi.org/10.1016/j.fuel.2008.07.011
[43] Soltic P, Hilfiker T. Efficiency and raw emission benefits from hydrogen addition to methane in a prechamber–equipped engine. Int J Hydrog Energy. 2020;45(43):23638-23652. https://doi.org/10.1016/j.ijhydene.2020.06.123
[44] Tang Q, Sampath R, Marquez ME, Sharma P, Hlaing P, Houidi MB et al. Optical diagnostics on the pre-chamber jet and main chamber ignition in the active pre-chamber combustion (PCC). Combust Flame. 2021;228:218-235. https://doi.org/10.1016/j.combustflame.2021.02.001
[45] The European Hydrogen Observatory. The European hydrogen market landscape. 2023. https://observatory.clean-hydrogen.europa.eu/
[46] Tomić R, Sjerić M, Krajnović J, Ugrinić S. Influence of pre-chamber volume, orifice diameter and orifice number on performance of pre-chamber SI engine – an experimental and numerical study. Energies. 2023;16(6):2884. https://doi.org/10.3390/en16062884
[47] Torres-Jimenez E, Jerman MS, Gregorc A, Lisec I, Dorado MP, Kegl B. Physical and chemical properties of ethanol–diesel fuel blends. Fuel. 2011;90(2):795-802. https://doi.org/10.1016/j.fuel.2010.09.045
[48] Tutak W, Jamrozik A. Modelling of the thermal cycle of a gas engine using AVL FIRE Software. Combust Engines. 2010;141(2):105-113. https://doi.org/10.19206/CE-117152
[49] Wang K da, Sun B gang, Luo Q he, Li Q, Wu X, Hu T et al. Performance optimization design of direct injection turbocharged hydrogen internal combustion engine. Appl Energy Combust Sci. 2023;16:100204. https://doi.org/10.1016/j.jaecs.2023.100204
[50] Wang Z, Ji C, Wang D, Zhang T, Wang S, Wang H et al. Analysis of the combustion characteristics of ammonia/air ignited by turbulent jet ignition with assisted hydrogen injection in pre-chamber. Fuel. 2024;367:131513. https://doi.org/10.1016/j.fuel.2024.131513
[51] White C, Steeper R, Lutz A. The hydrogen-fueled internal combustion engine: a technical review. Int J Hydrog Energy. 2006;31(10):1292-1305. https://doi.org/10.1016/j.ijhydene.2005.12.001
[52] Wu H, Wang L, Wang X, Sun B, Zhao Z, Lee C et al. The effect of turbulent jet induced by pre-chamber sparkplug on combustion characteristics of hydrogen-air pre-mixture. Int J Hydrog Energy. 2018;43(16):8116-8126. https://doi.org/10.1016/j.ijhydene.2018.02.155
[53] Xu G, Kotzagianni M, Kyrtatos P, Wright YM, Boulouchos K. Experimental and numerical investigations of the unscavenged prechamber combustion in a rapid compression and expansion machine under engine-like conditions. Combust Flame. 2019;204:68-84. https://doi.org/10.1016/j.combustflame.2019.01.025
[54] Zeman J, Dempsey A. Numerical investigation of equivalence ratio effects on flex-fuel mixing controlled combustion enabled by prechamber ignition. Appl Therm Eng. 2024; 249:123445. https://doi.org/10.1016/j.applthermaleng.2024.123445
[55] Zhou L, Liu P, Zhong L, Feng Z, Wei H. Experimental observation of lean flammability limits using turbulent jet ignition with auxiliary hydrogen and methane in prechamber. Fuel. 2021;305:121570. https://doi.org/10.1016/j.fuel.2021.121570
[56] Zhou L, Zhong L, Liu Z, Wei H. Toward highly-efficient combustion of ammonia–hydrogen engine: prechamber turbulent jet ignition. Fuel. 2023;352:129009. https://doi.org/10.1016/j.fuel.2023.129009
[57] Zhu J, Liu R, Lin H, Jin Z, Qian Y, Zhou D et al. Computational insights into flame development and emission formation in an ammonia engine with hydrogen-assisted prechamber turbulent jet ignition. Energy Convers Manag. 2024;314:118706. https://doi.org/10.1016/j.enconman.2024.118706
[58] Ziyaei S, Mazlan SK, Lappas P, Ziyaei S, Mazlan SK, Lappas P. A review of ultra-lean and stratified charged combustion in natural gas spark ignition engines. Technical Paper 2003-16-0050. 2023. https://doi.org/10.4271/03-16-07-0050

Marcelina Górzyńska, MEng. – Faculty of Civil and Transport Engineering, Poznan University of Technology, Poland.
e-mail: *marcelina.gorzynska@doctorate.put.poznan.pl*

Prof. Ireneusz Pielecha, DSc., DEng. – Faculty of Civil and Transport Engineering, Poznan University of Technology, Poland.
e-mail: *ireneusz.pielecha@put.poznan.pl*